Jpn. J. Infect. Dis., 69, 285–292, 2016

Original Article

Proteomic Profiling of a Respiratory Syncytial Virus-Infected Rat Pneumonia Model

Xue-Feng Wang[1†*], Xiu-Ying Zhang[2†], Xuejuan Gao[3†], Xiao-Xue Liu[2], and Yi-Huan Wang[2]

[1]The Affiliated Hospital of Liaoning University of Traditional Chinese Medicine, Liaoning; [2]The Graduate College of Liaoning University of Traditional Chinese Medicine, Liaoning; and [3]Key Laboratory of Functional Protein Research of Guangdong Higher Education Institutes, Institute of Life and Health Engineering, Jinan University, Guangdong, China

SUMMARY: Respiratory syncytial virus (RSV) is a major cause of lower respiratory tract disease in pediatric patients. Our goal was to obtain a detailed understanding of the molecular pathogenesis of RSV infections by studying the protein expression profiles in rats with pneumonia. First, we successfully established a pneumonia rat model by intranasally injecting RSV. The differentially expressed proteins in lung tissues of RSV-infected rats compared with those of the controls were analyzed by using 2-dimensional fluorescence difference gel electrophoresis and MALDI-TOF/TOF MS. In total. 41 differentially expressed protein spots representing 20 unique proteins were successfully identified. Classification analysis showed that most of these proteins are implicated in metabolic processes, cellular processes, cellular component organization or biogenesis, and immune system processes. The significantly elevated expressions levels of 4 proteins namely, T-kininogen 1, T-kininogen 2, haptoglobin, and hemopexin, which might serve as the potential biomarkers of RSV-infected pneumonia, were further validated in RSV-infected rats using western blot and immunohistochemistry. These results provide new insights into the pathogenesis of RSV infection-induced pneumonia and provide important future directions for functional studies and therapeutic design.

INTRODUCTION

Pneumonia, commonly caused by respiratory viral infections, is a leading cause of morbidity and mortality. Among the known causative viruses, the respiratory syncytial virus (RSV) is the chief pathogen responsible for most lower respiratory tract infections (community-acquired pneumonia or bronchiolitis) during infancy and early childhood, throughout developed and developing countries (1).

RSV is a single-stranded, negative-polarity RNA virus from the *Paramyxoviridae* family. The RSV genome encodes 11 proteins, including the small hydrophobic protein (SH), the attachment glycoprotein (G), and the fusion protein (F), which make up the viral protein coat. RSV infection does not provoke a lasting immunity (2), and repeated infection is common at all ages (3). Therapeutic options to combat these infections are limited and somewhat ineffective.

Since its discovery in 1956, no vaccine or effective treatment has been developed against RSV infection (4). Approximately 25% to 40% of first exposures to RSV result in symptoms of bronchiolitis or pneumonia. Approximately 65% of all children are infected with RSV within the first year of life, and almost all children are infected at least once by the age of 2 years; thus, RSV infection causes 160,000–600,000 deaths per year (5–7). Nosocomial RSV infection in children is associated with a higher mortality than that associated with a community-acquired illness because of pre-existing morbidity (8,9). Elderly or adult patients with chronic pulmonary disease or weakened immune systems are at a high risk of developing severe RSV disease (10).

However, the underlying mechanisms responsible for the interactions between RSV infection and the development of pneumonia are not clearly understood. In general, animal disease models provide opportunities to elucidate of the underlying mechanisms and potential therapeutic interventions. Owing to the difference in consequences of RSV-induced pneumonia, especially between predisposed atopic and non-atopic infants, animal models are often used to mimic clinical conditions.

Here, we used Sprague-Dawley (SD) rats infected with RSV to establish a rat model for pneumonia in order to elucidate the mechanisms underlying the association between early, severe RSV infection and the development of pneumonia later in childhood. We investigated the proteome of the lung tissue from rats infected with RSV and healthy rats by using two-dimensional fluorescence difference gel electrophoresis (2D-DIGE) and identified the protein using matrix-assisted laser desorption/ionization time of flight mass spectrometry/time of flight mass spectrometry (MALDI-TOF/TOF MS).

This study is the first to employ proteomics with subsequent bioinformatics in the investigation of the proteomic profile of an RSV-infected rat model system.

Received May 29, 2015. Accepted July 24, 2015. J-STAGE Advance Publication September 11, 2015.
DOI: 10.7883/yoken.JJID.2015.244

†These authors contributed equally to this work.

*Corresponding author: Mailing address: The Affiliated Hospital of Liaoning University of Traditional Chinese Medicine, Shenyang 110032, Liaoning, China. Tel: +86-2431961175, Fax: +86-2431961175, E-mail: pcxwxf2015@163.com

After initial protein identification, we performed related analyses to find differences in the underlying protein pathways associated with pneumonia. Our goal was to obtain a detailed understanding of the changes in differentially expressed proteins in tissues associated with pneumonia in a rat model system.

MATERIALS AND METHODS

RSV preparation: The Long strain of RSV was obtained from the Capital Institute of Pediatrics and stored in the virus laboratory at the Department of Pediatrics of the Affiliated Hospital of Liaoning University of Traditional Chinese Medicine. The virus was propagated in Hep-2 cells, and infectious RSV titers were determined by measuring the 50% tissue culture infective dose ($TCID_{50}$). The viral pools were divided into aliquots, flash-frozen in liquid nitrogen, and stored at −80°C until used.

Infection of rats and lung tissue isolation: Male SD rats (weight range, 80–100 g; age, 4–6 weeks) were purchased from the Experimental Animal Center of Liaoning University of Traditional Chinese Medicine. All rats were housed individually under controlled conditions (specific pathogen-free) and fed sterilized water and food *ad libitum*. All experimental procedures involving rats were approved by the Institutional Animal Care and Use Committee.

Six SD rats were inoculated intranasally under ethyl ether with 100 μL of RSV suspension for 3 consecutive days to generate the rat pneumonia model (RPM). For control experiments, 6 healthy SD rats inoculated intranasally with vehicle under ethyl ether were used. The rats were killed by cervical dislocation 7 days post-infection for experimental and control groups. Post-mortem, the thorax was opened and the lungs were examined for gross lesions. The lungs were then removed for tissue collection. The left lung lobe was taken for histopathological staining and immunohistochemical analysis. The right lung lobe was taken for reverse transcription PCR (RT-PCR), proteomic analysis, and western blot assays. All tissue samples were flash-frozen in liquid nitrogen after dissection.

RT-PCR: Total RNA was extracted from the lung tissue samples of controls and RPM groups using TRIzol (Invitrogen, Carlsbad, CA, USA). The isolated RNA was treated with DNase and the cDNA was synthesized using SuperScript reverse transcriptase (Invitrogen). PCR amplification was performed with a 1 μL cDNA sample; the optimal annealing temperature and number of amplifications were determined for the primers of the RSV F gene, and PCR products were obtained within the linear range of amplification. GAPDH was set as a reference gene. The resulting PCR products were separated by electrophoresis on 2.0% agarose gels and visualized under ultraviolet light.

Histopathological staining: The tissue samples were fixed in 10% neutral formalin buffered solution, gradient dehydrated with alcohol, embedded in paraffin, and cut into 4 μm tissue sections. The sections were dried, dewaxed, gradient hydrated with alcohol, stained with hematoxylin and eosin (HE), and observed for pathological characteristics under a microscope.

Protein labeling with CyDye DIGE fluorophores: Protein extracts were labeled with 3 CyDye DIGE fluorophores, Cy2, Cy3, and Cy5, for 2-D DIGE technology according to the manufacturer's recommended protocols (GE Healthcare, Piscataway, NJ, USA). In total, 50 μg of protein from a pooled sample comprising of equal amounts of each of the 6 control samples was labeled with 400 pmol of Cy3, and 50 μg of protein from a pooled sample consisting of equal amounts of each of the 6 RPM samples was labeled with 400 pmol of Cy5. An internal reference standard, comprising 2 mixed samples that were used in the experiment, was labeled with Cy2. The labeling reaction was incubated on ice for 30 min in the dark. The reactions were then quenched with the addition of 10 mM lysine for 10 min on ice in the dark. The labeled samples were pooled and prepared for the subsequent steps of the experiment.

2-D electrophoresis: 2-D electrophoresis was performed as described earlier with a few minor modifications (11). Immobilized pH gradient (IPG) strips (24 cm, pH 4–7) were hydrated in hydration buffer (7 M urea, 2 M thiourea, 4% [w/v] 3-[(3-Cholamidopropyl) dimethylammonio] propanesulfonate [CHAPS], 40 mM dithiothreitol [DTT], 1% IPG buffer, pH 4–7, and 0.002% [w/v] bromophenol blue), and isoelectric focusing (IEF) was performed according to the manufacturer's instructions using pH 4–7 IPG strips with an Ettan IPGphor II System (GE Healthcare). After the IEF, the proteins were reduced and alkylated by successive treatment for 15 min with equilibration buffer containing 2% (w/v) DTT followed by 2.5% (w/v) iodoacetamide. Second-dimension separation was performed on a 12.5% SDS-PAGE gel using an Ettan DALTsix instrument (GE Healthcare).

Gel image acquisition and analysis: Labeled proteins were visualized using the Typhoon 9400 imager (GE Healthcare) (12,13). Briefly, the Cy2-, Cy3-, and Cy5-labeled images for each gel were scanned with excitation/emission wavelengths of 488/520, 532/580 and 633/670 nm, respectively. After the CyDye labeling, signals were imaged, and the gels were stained using Deep Purple total protein stain (GE Healthcare) according to the standard protocol and scanned with the excitation/emission wavelengths of 532/560 nm. Then, the 2-D DIGE gel images were analyzed using DeCyder 2D (Ver. 6.0; GE Healthcare) as described previously (12,13). The protein expression patterns of RSV lung tissue samples were compared with the controls. Protein spots with significant differences in abundance (more than 1.5-fold) (14) were selected for spot picking.

Spot picking and enzymatic digestion: Protein spot-features that were significantly ($p < 0.05$) increased or decreased in RSV model samples compared with control samples were chosen for further analysis. Two preparative gels were performed to enable recovery of sufficient protein within the individual spot feature to allow protein identification. In the automated procedure, the selected protein spots were picked up, washed with 25 mM NH_4HCO_3 and 50% (v/v) methanol, and then digested with 20 ng/μL trypsin (sequencing-grade; Promega, Madison, WI, USA) in 25 mM NH_4HCO_3 for 12 h at 37°C. The tryptic peptides were extracted with 60% (v/v) Acetonitrile (ACN) and 0.1% (v/v) trifluoroacetic acid (TFA), dissolved in 4 mg/mL α-cyano-4-hydroxycinnamic acid (CHCA) matrix in 70% (v/v)

ACN and 0.1% (v/v) TFA, and spotted on the MS sample plate.

MALDI-TOF/TOF MS analysis: MS analysis was performed on an Ultraflex III MALDI-TOF/TOF MS (Bruker, Karlsruhe, Germany) operating in the positive ion reflector mode. Monoisotopic peak masses were acquired in the mass range of 700–3,200 Da with a signal-to-noise ratio (S/N) >200. Four of the most intense ion signals, excluding common trypsin autolysis peaks and matrix ion signals, were automatically selected as precursors for MS/MS acquisition.

Database searching: The peptide mass fingerprints (PMF) combined MS/MS spectra were searched against the NCBInr database using the Biotools software (Ver. 3.2; Bruker) and Mascot (Ver. 2.2; Matrix Science, Boston, MA, USA) with the following parameters to identify the proteins in *Rattus* protein databases; trypsin digest (one missing cleavage allowed), carbamidomethylation as fixed modification, oxidation of methionines allowed as variable modification, peptide mass tolerance at 50 ppm, fragment tolerance at 0.6 Da, mass value: monoisotropic, and protein mass ranged from 1 to 100 kDa. UniProt databases were searched. Mascot protein scores (based on combined MS and MS/MS spectra) of greater than 65 were considered statistically significant ($p < 0.05$).

Western blotting: Western blotting was performed on every lung extraction from RSV-infected and control rats. Briefly, 50 μg of protein extracts from each group were separated by SDS-PAGE (12–15% acrylamide) and then transferred onto polyvinylidene difluoride (PVDF) membranes. The membranes were incubated with anti-T-kininogen 1 (KNT1), anti-T-kininogen 2 (KNT2), anti-haptoglobin (HP), anti-hemopexin (HPX), and anti-GAPDH (internal reference) antibodies at 4°C overnight, followed by incubation with horseradish peroxidase-conjugated secondary antibodies at room temperature for 2 h. Specific protein bands were visualized using the SuperSignal chemiluminescence system (ECL; Pierce, Waltham, MA, USA) and imaged onto X-ray film.

Immunohistochemistry: Immunohistochemical staining was performed using various primary antibodies including anti-KNT1, anti-KNT2, anti-HP, and anti-HPX, as previously described (15). These antibodies are the same as those used in western blotting. Two experienced pathologists assessed the immunostaining in a blinded fashion as previously described (16). Immunohistochemical staining was assessed semi-quantitatively by measuring the extent of staining (0, 0%; 1, 0–10%; 2, 10–50%; and 3, 50–100%) as well as the intensity of staining (0, no staining; 1, yellow; 2, brown to yellow; and 3, brown staining). The scores for extent and intensity of staining for each case were multiplied to obtain weighted scores (0, negative [−]; 1–4, weakly positive [+]; 5–8, moderately positive [++]; and 9–12, strongly positive [+++]). The weighted scores of 0–4 were considered as negative and 5–12 as positive.

Protein categorization and network construction: Identified proteins were classified based on the Protein ANalysis THrough Evolutionary Relationships (PANTHER) system <http://www.pantherdb.org>, a unique resource that classifies genes and proteins by their functions (17,18). The PANTHER ontology, a highly controlled vocabulary (ontological terms) by molecular function, protein class, and biological process was used to categorize proteins into families and subfamilies with shared functions. The interaction network of the differentially expressed proteins was generated using Pathway Studio Version 5.0 software (Ariadne Genomics, Rockville, MD, USA) and Resnet 5 database. Common upstream regulators or downstream targets of multiple proteins were identified with this software, facilitating the process of selecting potential mechanisms and key factors from the large number of differentially regulated proteins.

RESULTS

Verification of the RPM by RSV infection: RSV infection was assessed by performing RT-PCR on homogenized lung tissues of rats from control and RPM groups. As RSV F mRNA was detected at day 3, 5, and 7, following RSV infection in these tissues and was not detected in control, rats from the RPM group were determined to have been successfully infected by RSV (Fig. 1A). Subsequently, the hematoxylin eosin (HE) staining was performed on the lung slices of the RSV-infected and control rats to test the characteristics of RSV-induced pneumonia. As shown in Fig. 1B, alveolar septum thickening, extensive lymphocyte and monocyte infiltration, and typical pulmonary interstitial pneumonia were observed in the experimental group, but not in the control group. These results suggested that intranasal inoculation of the RSV suspension successfully caused typical pneumonia in the rats (Fig. 1B).

Identification of differential protein expression in lung tissue of rats from the RPM group: Protein extracts from tissue homogenates were subjected to 2D-DIGE analysis to investigate the potential changes in the rat lung in response to infection with RSV (Fig. 2). To our knowledge, no previous study has identified proteome changes in lung tissue infected with RSV. As shown in Fig. 2, the red spots represent up-regulated proteins, and green spots represent down-regulated proteins in RPM samples compared to control samples. The arrows point to the proteins that exhibited significantly differential expression between RPM and control samples. A 1.5-fold cutoff (14) was chosen as a basis for investigating potential protein expression differences between data sets and to provide a basis for comparing the current data set with other studies. A total of 41 differentially expressed protein spots (4 down-regulated and 37 up-regulated) representing 20 unique proteins were successfully identified in the RPM samples compared to control samples (Table 1). Some proteins appeared at multiple spots in DIGE, likely due to protein isoforms and/or modifications.

The KNT1, an inhibitor of cysteine proteinase, presented the highest ratio (RPM/C) of 9.79536 in these identified proteins (Table 1). KNT1 and KNT2 are precursors of pro-inflammatory vasoactive kinins and may participate in anti-inflammatory pathways through the inhibition of cysteine proteinases (19,20).

Functional categories and biological interaction network of the identified differentially expressed proteins: In order to understand the biological relevance of the changes in protein expression in the RPM samples, the

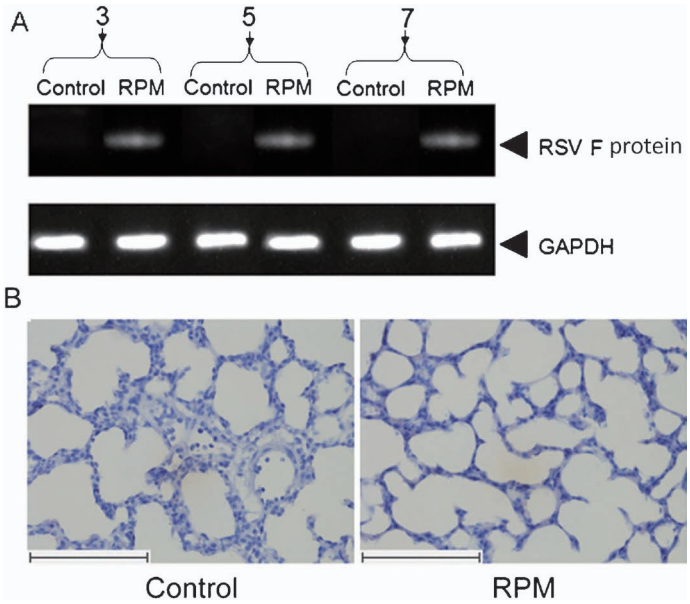

Fig. 1. (Color online) Verification of the rat pneumonia model (RPM) generated by infection with respiratory syncytial virus (RSV). (A) Confirmation of the RSV infection at day 3, 5, and 7 after infection in rats. RSV F protein mRNA was amplified by RT-PCR from lung tissue samples of RPM and control groups. (B) Histopathological staining indicated alveolar septum thickening and extensive lymphocyte and monocyte infiltration in the RPM rat lungs. The typical results of histopathology staining are represented. Scale bar: 100 μm.

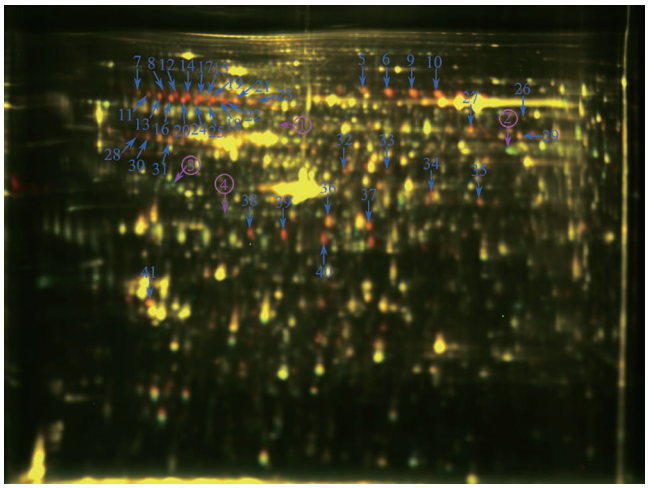

Fig. 2. (Color online) Representative DIGE gel image of differentially expressed proteins in tissue samples of RPM. Proteins extracted from RPM and control samples were labeled with Cy3 and Cy5, respectively. An internal standard protein sample (a mixture of RPM and control samples) was labeled with the Cy2 dye. The green spots represent down-regulated proteins (encircled numbers), while the red spots represent up-regulated proteins in RPM samples compared with control samples. Arrows indicate the proteins that exhibited significantly differential expression between RPM and control samples. Each number of the arrow corresponds to each protein presented in Table 1.

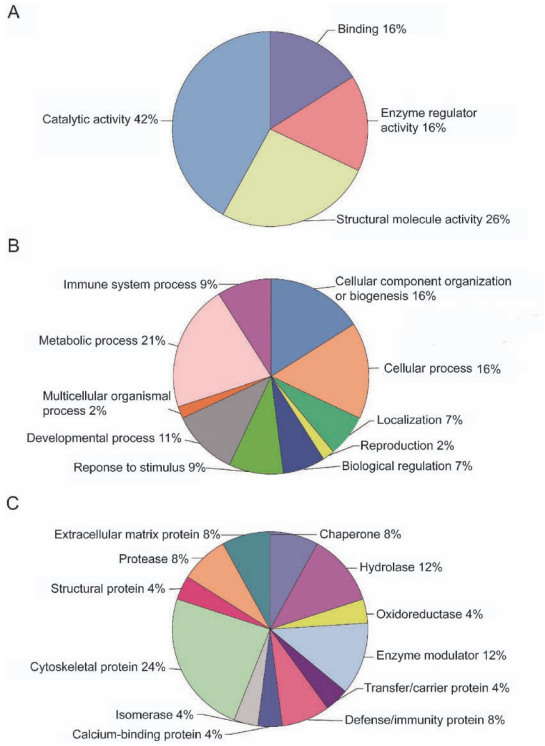

Fig. 3. (Color online) Classification analysis of differentially expressed proteins identified in the lung tissue samples from the RPM. Categorization was obtained from the online PANTHER classification system. (A) Classification of the differentially expressed proteins according to molecular function. (B) Classification of the differentially expressed proteins according to biological process. (C) Classification of the differentially expressed proteins according to protein class.

PANTHER system was used to categorize the identified proteins according to their molecular function, biological process, and protein class. The most dominant molecular function that the identified proteins were involved in was catalytic activity (42%), followed by structural molecule activity (26%), enzyme regulator ac-

Table 1. Identification of differentially expressed proteins from the RSV-infected RPM group compared to the control group

Spot No.	Protein name	Accession No.	Protein score	Protein MW (Da)	Protein PI	Sequence coverage (%)	Ratio (RPM/C)
①	Alpha-2-HS-glycoprotein	P24090	163	38,757	6.05	0.22	−1.64428
②	Aldehyde dehydrogenase, mitochondrial	P11884	349	56,966	6.63	0.31	−1.67018
③	Vimentin	P31000	287	53,757	5.06	0.43	−1.83231
④	Heat shock cognate 71 kDa protein	P63018	138	71,055	5.37	0.11	−1.66311
5	HPX (Hemopexin)	P20059	164	52,060	7.58	0.22	1.88850
6	HPX	P20059	494	52,060	7.58	0.31	2.43651
7	KNT2 (T-kininogen 2)	P08932	107	48,757	5.94	0.10	1.60604
8	KNT1 (T-kininogen 1)	P01048	92	48,828	6.08	0.11	7.94589
9	HPX	P20059	300	52,060	7.58	0.26	2.93319
10	HPX	P20059	380	52,060	7.58	0.29	2.10955
11	KNT2	P08932	165	48,757	5.94	0.10	2.37683
12	KNT1	P01048	132	48,828	6.08	0.07	6.50020
13	KNT2	P08932	100	48,757	5.94	0.10	2.90280
14	KNT1	P01048	91	48,828	6.08	0.07	5.78302
15	KNT1	P01048	159	48,828	6.08	0.07	1.50000
16	KNT2	P08932	155	48,757	5.94	0.10	2.95381
17	KNT1	P01048	97	48,828	6.08	0.05	5.92857
18	KNT1	P01048	186	48,828	6.08	0.10	2.27421
19	KNT1	P01048	141	48,828	6.08	0.12	6.50232
20	KNT2	P08932	133	48,757	5.94	0.10	3.96070
21	KNT1	P01048	168	48,828	6.08	0.09	1.88957
22	KNT1	P01048	136	48,828	6.08	0.10	9.79536
23	KNT1	P01048	122	48,828	6.08	0.07	1.50640
24	KNT2	P08932	153	48,757	5.94	0.13	4.98111
25	KNT2	P08932	73	48,757	5.94	0.09	5.04633
26	Moesin	O35763	140	67,868	6.16	0.18	1.53581
27	Protein disulfide-isomerase A3	P11598	353	57,044	5.88	0.30	2.17840
28	Serine protease inhibitor A3N	P09006	184	46,793	5.33	0.25	1.87650
29	Coronin-1A	Q91ZN1	100	51,717	6.05	0.20	1.64393
30	Serine protease inhibitor A3N	P09006	218	46,793	5.33	0.25	2.15443
31	Endoplasmin	Q66HD0	178	92,998	4.72	0.16	1.62859
32	Ezrin	P31977	135	69,462	5.83	0.19	2.36290
33	Guanine deaminase	Q9WTT6	227	51,554	5.56	0.29	1.55701
34	Pyruvate kinase isozymes M1/M2	P11980	235	58,294	6.63	0.25	2.06010
35	Leukocyte elastase inhibitor A	Q4G075	227	42,871	5.92	0.24	1.75584
36	Actin, cytoplasmic 1	P60711	175	42,052	5.29	0.18	1.63538
37	Actin, cytoplasmic 2	P63259	62	42,108	5.31	0.20	1.71067
38	Haptoglobin (HP)	P06866	188	39,052	6.10	0.24	2.51877
39	HP	P06866	177	39,052	6.10	0.22	3.39014
40	HP	P06866	155	39,052	6.10	0.24	2.84378
41	C-reactive protein	P48199	40	25,737	4.89	0.07	1.64034

MW, molecular weight; PI, isoelectric point; RPM, rat pneumonia model; C, control.

tivity (16%), and binding (16%) (Fig. 3A). All proteins could be mapped to this system except for KNT2. However, KNT1 and KNT2 are known to have almost identical functions. Most of these proteins participated in metabolic processes (21%), cellular processes (16%), cellular component organization or biogenesis (16%), immune system process (9%), and response to stimulus (9%). The proteins were also involved in other biological processes, such as developmental process, biological regulation, localization, multicellular organism processes, and reproduction (Fig. 3B). The involvement of ''immune system process'' suggests that the expression levels of proteins involved in the immune response were elevated and that the immune response in the lung of RSV-infected rats was activated. The proteins were classified into 12 groups based on protein class. The most prevalent proteins were cytoskeletal proteins (24%), followed by enzyme modulators (12%) and hydrolases (12%). In addition, there were other proteins including defense/immunity proteins (8%), extracellular matrix proteins (8%), proteases (8%), chaperones (8%), and oxidoreductases (4%) (Fig. 3C).

To explore the associations between the differentially expressed proteins, we constructed a protein network using the Pathway Studio 5.0 software (Scientific Computing, Rockway, NJ, USA) (21). Complex interactions between mitochondrial, nuclear, cytoplasmic, and extracellular proteins were present in the predicted network (Fig. 4), which includes nuclear receptors, kinases, phosphatases, extracellular proteins, ligands,

transcription factors, and receptors. The identified proteins constructed a complex network related to inflammatory processes through interacting with other protein nodes. The four most differentially expressed proteins KNT1, (KNT2; has almost identical functions with KNT1), HPX, and HP are indicated in Fig. 4 with red arrows.

Validation of differentially expressed proteins by western blotting and immunohistochemistry: To confirm the proteomic results further, western blotting was performed to examine the expression levels of KNT1, KNT2, HPX, and HP (the 4 most differentially expressed proteins) in protein extracts from RPM and control lungs. Western blot analysis showed that the expression levels of these 4 proteins were higher in the RPM group than in the control group (Fig. 5A), consistent with the 2D-DIGE analysis and the proteomic assay (Table 1). Simultaneously, immunohistochemical staining was performed to examine the expression levels of KNT1, KNT2, HPX, and HP proteins in lung samples of rats from RPM and control groups. The results showed that the RPM group had significantly higher expression of these proteins than the control group (Fig. 5B). Similar results were obtained for all 6 rats, and 1 representative example is shown.

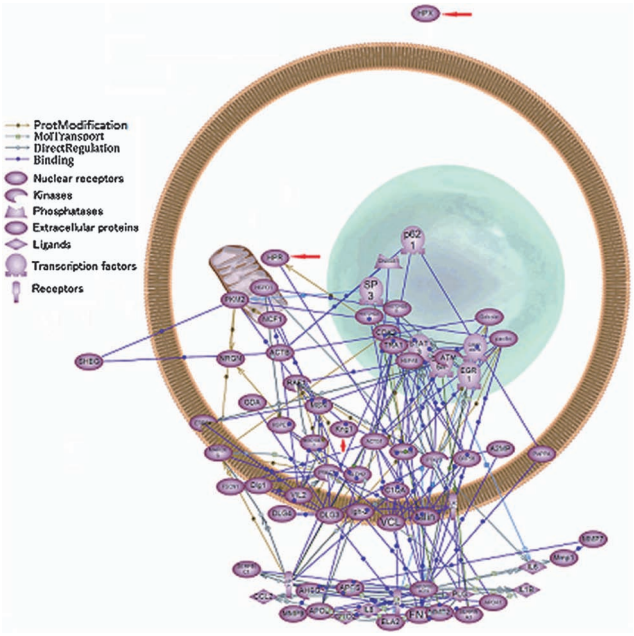

Fig. 4. (Color online) Protein network analysis of the RPM. Proteins shown in Table 1 were imported into Pathway Assist, and an interaction map was created. Each node represents either a protein entity or a control mechanism of the interaction. Proteins that either bound directly to another identified protein or to another identified protein via one other protein are shown. The arrows indicate the proteins of KNT1 (Kng1), HP (HPR), and HPX.

DISCUSSION

In the present study, we used a proteomic approach to determine the underlying pathogenesis in an RPM. Specifically, we defined a set of differentially expressed proteins that could be used to facilitate diagnosis and develop therapeutics. The identification of these differentially expressed proteins helped us to gain a deeper understanding of the early pathological processes associated with pneumonia.

To the best of our knowledge, changes in protein expression due to pneumonia caused by RSV infections have not been previously reported. Using 2D-DIGE-based proteomics, we identified 41 differentially expressed proteins in lung tissue samples from RPM and compared them with healthy controls. Of these proteins, the 4 most significantly and differentially expressed proteins KNT1, KNT2, HP, and HPX were validated by western blotting and immunohistochemistry. KNT1 and KNT2, inhibitors of cysteine proteinases, have been shown to participate in inflammatory processes. For example, the allergic lung inflammation of human asthma in a mouse model can be prevented by using the extracellular cysteine protease inhibitor E64 (22). KNT also played a role in immunosenescence through inhibition of extracellular signal-regulated kinase (ERK)-dependent T cell proliferation (23). A recent report showed that the anti-inflammatory agents, curcumin and capsaicin, prevented the acute-phase inflammatory response of arthritis partly through the

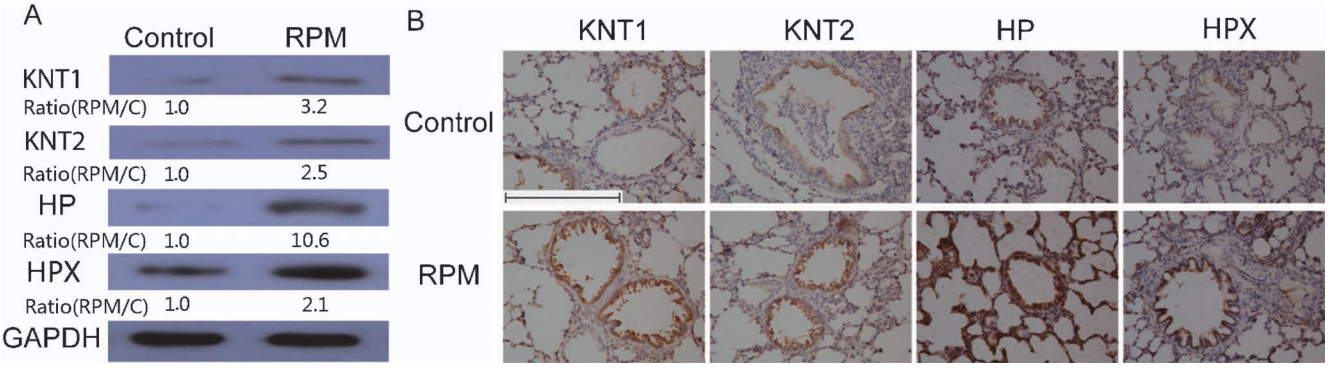

Fig. 5. (Color online) Verification of proteomic analysis. (A) Western blot validation of 4 proteins (KNT1, KNT2, HP, and HPX) in RPM and control samples. GAPDH was used as the internal reference. The ratios of RPM to control (C) represent the changing trends of the corresponding proteins expressed in RPM group compared to that in control group (below the bands of corresponding protein). (B) Representative results of immunohistochemical staining of KNT1, KNT2, HP, and HPX in RPM and control lung tissues. Scale bar: 100 μm.

down-regulation of KNT1 (24). These reports suggested that the apparent up-regulation of KNT1 in the RSV-infected rats facilitated disease progression, implied the generation of inflammation response in the lung of RSV-infected rats, and that the KNT1 might be a potential target of RSV-infected pneumonia therapy. Another elevated protein, HP, has been reported to be associated with LPC-2, as a biomarker to help distinguish the etiology of clinical pneumonia (25). Furthermore, the expression of HP has been found to be increased using 2-D gel electrophoresis and MS analysis, and HP may also play a role in the development of chronic hypersensitivity pneumonitis (26). HPX, a serum glycoprotein, associates with heme and transports it to the liver for decomposition and iron recovery. HPX, together with HP and transferrin, forms the 4th most abundant group of plasma proteins. They act as antioxidants by binding heme strongly (27). The heme complexes with HPX, HP, or albumin show a much lower peroxidase- and catalase-like activity than the non-protein bound heme (28). Therefore, we speculate that up-regulation of HPX and HP may play a significant role in the pathogenesis of pneumonia and could be used as a potential drug target.

The association of another protein, ezrin (EZR), with pneumonia has not been reported. In our study, the expression of EZR was significantly elevated in the lung tissue samples of RPM (Table 1, RPM/C: 2.3629). EZR is a member of the ERM family (including ezrin, radixin, and moesin) and is involved in the connections of major cytoskeletal structures to the plasma membrane. ERM family proteins regulate many cellular processes, can be phosphorylated upon stimulation of cells with the proinflammatory cytokine, tumor necrosis factor-α (TNF-α) and are involved in the modulation of TNF-α-induced endothelial permeability (29). This report suggested that EZR might participate in the development of RSV-induced pneumonia.

In addition, protein extracts from 6 lung tissues of each group were used to perform 2D-DIGE and MALDI-TOF/TOF MS assay in our study. The design is a conventional strategy for proteomics analysis. By using 6 pooled samples, repeatability and reliability were guaranteed, so that the instability and extremes of a single sample did not skew the results. Furthermore, the experimental costs of MS analysis were reduced.

In summary, this study is the first to employ proteomics with subsequent bioinformatics analysis in the investigation of a rat model of RSV-induced pneumonia. The identified differentially expressed proteins provide useful information for understanding and elaborating the pathogenesis of RSV infection-induced pneumonia. Further research is needed to explore the role of these proteins and their interactions in the mechanism of pneumonia caused by RSV infection.

Acknowledgments This work was supported by National Natural Science Foundation (81273800).

Conflict of interest None to declare.

REFERENCES

1. Bawage SS, Tiwari PM, Pillai S, et al. Recent advances in diagnosis, prevention, and treatment of human respiratory syncytial virus. Adv Virol. 2013;2013:595768.
2. Singleton R, Etchart N, Hou S, et al. Inability to evoke a long-lasting protective immune response to respiratory syncytial virus infection in mice correlates with ineffective nasal antibody responses. J Virol. 2003;77:11303-11.
3. Pockett RD, Campbell D, Carroll S, et al. Rotavirus, respiratory syncytial virus and non-rotaviral gastroenteritis analysis of hospital readmissions in England and Wales. Acta Paediatr. 2013;102: e158-63.
4. Hall CB. Respiratory syncytial virus and parainfluenza virus. N Engl J Med. 2001;344:1917-28.
5. Bloom-Feshbach K, Alonso WJ, Charu V, et al. Latitudinal variations in seasonal activity of influenza and respiratory syncytial virus (RSV): a global comparative review. PLoS One. 2013;8: e54445.
6. Henrickson KJ. Cost-effective use of rapid diagnostic techniques in the treatment and prevention of viral respiratory infections. Pediatr Ann. 2005;34:24-31.
7. Krilov LR. Respiratory syncytial virus disease: update on treatment and prevention. Expert Rev Anti Infect Ther. 2011;9:27-32.
8. Langley JM, LeBlanc JC, Wang EE, et al. Nosocomial respiratory syncytial virus infection in Canadian pediatric hospitals: a Pediatric Investigators Collaborative Network on Infections in Canada Study. Pediatrics. 1997;100:943-6.
9. Simon A, Muller A, Khurana K, et al. Nosocomial infection: a risk factor for a complicated course in children with respiratory syncytial virus infection--results from a prospective multicenter German surveillance study. Int J Hyg Environ Health. 2008;211: 241-50.
10. Falsey AR, Hennessey PA, Formica MA, et al. Respiratory syncytial virus infection in elderly and high-risk adults. N Engl J Med. 2005;352:1749-59.
11. Liang CR, Leow CK, Neo JC, et al. Proteome analysis of human hepatocellular carcinoma tissues by two-dimensional difference gel electrophoresis and mass spectrometry. Proteomics. 2005;5: 2258-71.
12. Jin S, Shen JN, Guo QC, et al. 2-D DIGE and MALDI-TOF-MS analysis of the serum proteome in human osteosarcoma. Proteomics Clin Appl. 2007;1:272-85.
13. Fu H, Li W, Liu Y, et al. Mitochondrial proteomic analysis and characterization of the intracellular mechanisms of bis(7)-tacrine in protecting against glutamate-induced excitotoxicity in primary cultured neurons. J Proteome Res. 2007;6:2435-46.
14. Canals F, Colome N, Ferrer C, et al. Identification of substrates of the extracellular protease ADAMTS1 by DIGE proteomic analysis. Proteomics. 2006;Suppl 1:S28-35.
15. Pang J, Liu WP, Liu XP, et al. Profiling protein markers associated with lymph node metastasis in prostate cancer by DIGE-based proteomics analysis. J Proteome Res. 2010;9:216-26.
16. Cheng AL, Huang WG, Chen ZC, et al. Identification of novel nasopharyngeal carcinoma biomarkers by laser capture microdissection and proteomic analysis. Clin Cancer Res. 2008;14:435-45.
17. Mi H, Guo N, Kejariwal A, et al. PANTHER version 6: protein sequence and function evolution data with expanded representation of biological pathways. Nucleic Acids Res. 2007;35:D247-52.
18. Thomas PD, Campbell MJ, Kejariwal A, et al. PANTHER: a library of protein families and subfamilies indexed by function. Genome Res. 2003;13:2129-41.
19. Kato H, Nakanishi E, Enjyoji K, et al. Characterization of serine proteinases isolated from rat submaxillary gland: with special reference to the degradation of rat kininogens by these enzymes. J Biochem. 1987;102:1389-404.
20. Enjyoji K, Kato H, Hayashi I, et al. Purification and characterization of rat T-kininogens isolated from plasma of adjuvant-treated rats. Identification of three kinds of T-kininogens. J Biol Chem. 1988;263:973-9.
21. Xiao CL, Zhang ZP, Xiong S, et al. Comparative proteomic analysis to discover potential therapeutic targets in human multiple myeloma. Proteomics Clin Appl. 2009;3:1348-60.
22. Layton GT, Harris SJ, Bland FA, et al. Therapeutic effects of cysteine protease inhibition in allergic lung inflammation: inhibition of allergen-specific T lymphocyte migration. Inflamm Res. 2001;50:400-8.
23. Acuña-Castillo C, Aravena M, Leiva-Salcedo E, et al. T-kininogen, a cystatin-like molecule, inhibits ERK-dependent lymphocyte proliferation. Mech Ageing Dev. 2005;126:1284-91.
24. Joe B, Nagaraju A, Gowda LR, et al. Mass-spectrometric iden-

tification of T-kininogen I/thiostatin as an acute-phase inflammatory protein suppressed by curcumin and capsaicin. PLoS One. 2014;9:e107565.
25. Huang H, Ideh RC, Gitau E, et al. Discovery and validation of biomarkers to guide clinical management of pneumonia in African children. Clin Infect Dis. 2014;58:1707-15.
26. Okamoto T, Miyazaki Y, Shirahama R, et al. Proteome analysis of bronchoalveolar lavage fluid in chronic hypersensitivity pneumonitis. Allergol Int. 2012;61:83-92.
27. Gutteridge JM. Lipid peroxidation and antioxidants as biomarkers of tissue damage. Clin Chem. 1995;41:1819-28.
28. Grinberg LN, O'Brien PJ, Hrkal Z. The effects of heme-binding proteins on the peroxidative and catalatic activities of hemin. Free Radic Biol Med. 1999;27:214-9.
29. Koss M, Pfeiffer GR, Wang Y, et al. Ezrin/radixin/moesin proteins are phosphorylated by TNF-alpha and modulate permeability increases in human pulmonary microvascular endothelial cells. J Immunol. 2006;176:1218-27.